Robotica (2016) volume 34, pp. 1168–1185. © Cambridge University Press 2014
doi:10.1017/S0263574714002161

Development and experimental evaluation of multi-fingered robot hand with adaptive impedance control for unknown environment grasping

Ting Zhang†, ‡, Li Jiang‡*, Shaowei Fan‡, Xinyu Wu† and Wei Feng†

†*Guangdong Provincial Key Laboratory of Robotics and Intelligent System, Shenzhen Institutes of Advanced Technology, Chinese Academy of Sciences, Shenzhen, P. R. China*
‡*State Key Laboratory of Robotics and System, Harbin Institute of Technology, Harbin, P. R. China*

(Accepted November 22, 2013. First published online: August 27, 2014)

SUMMARY
This paper presents adaptive impedance controllers with adaptive sliding mode friction compensation for anthropomorphic artificial hand. A five-fingered anthropomorphic artificial hand with multi-sensory and Field-Programmable Gate Arra (FPGA)-based control hardware and software architecture is designed to fulfill the requirements of the grasping force controller. In order to improve the force-tracking precision, the indirect adaptive algorithm was applied to estimate the parameters of the environment. The generalized momentum-based disturbance observer was applied to estimate the contact force from the torque sensor. Based on the sensors of the finger, an adaptive sliding mode friction compensation algorithm was utilized to improve the accuracy of the position control. The performances of the force-tracking impedance controller and position-based joint impedance control for the five-fingered anthropomorphic artificial hand are analyzed and compared in this paper. Furthermore, the performances of the force-tracking impedance controller with environmental parameters adaptive estimation and without environmental parameters estimation are analyzed and compared. Experimental results prove that accurate force-tracking and stable torque/force response under uncertain environments of unknown stiffness and position can be achieved with the proposed adaptive force-tracking impedance controller with friction compensation on five-finger artificial hand.

KEYWORDS: Multi-fingered robot hand; Adaptive impedance control; Blind environment grasping; Force control.

1. Introduction

Researchers have made numerous attempts at duplicating the form and function of the human hand. Numerous multi-fingered robot hands have been developed mainly in two categories: dexterous robot hand (e.g., the Gifu Hand[1] and the DLR/HIT Hand[2]) and prosthetic hand (e.g., CyberHand,[3] Manushand,[4] Smarthand,[5] DARPA hand,[6] multi-fingered robot hand,[7–11] iCub Humanoid Robot,[12] HIT prosthetic hand[13–15]). An essential feature of an anthropomorphic artificial hand is the capability to keep hold of manipulated objects despite disturbances, while maintaining compliance between the robot finger and the object to avoid damage to the hand and object. Stable grasp of objects by a dexterous robot hand or prosthetic hand is a complex subject that involves many factors: hand kinematics and dynamics, sensory feedback, object geometry, gravitational and translational acceleration forces, and environmental relationships between the hand and object (e.g., static coefficient of friction and fingertip deformation).[16] Real-time control fingertip grasp force is the basic task for stable grasp.

The impedance force control method has been known as one of major force control algorithms that can deal with environment by considering the relationship between the robot and the environment.[17] Hogan[18] introduced a framework for impedance control, which can be used to achieve compliant

* Corresponding author. E-mail: tzhang217@aliyun.com

https://doi.org/10.1017/S0263574714002161 Published online by Cambridge University Press

manipulation and reliable grasping with different objects in unknown environments. Impedance control on robot manipulators has been addressed by numerous literatures. Biagiotti[19] designed an admittance controller for the dexterous robot hand DLR II with a local proportional regulator in joint space to deal with singularity conditions of the kinematic structure. Wei *et al*.[20] developed an impedance controller for multi-finger dexterous robot hand DLR-HIT I together with the hardware and software architecture designs. Although the dynamic relationship is considered, one weak point of the impedance control method is the lack of the direct force control capability by specifying a desired force, which the hybrid force position control method has.[21] Therefore, the lack of force-tracking capability of the impedance control method has been paid attention by many researchers to solve the direct force control capability. Force-tracking impedance control is one of the main force control algorithms in the literature with the hybrid position and force control.[22] After the pioneering work of the impedance control by Hogan, there have been several major research issues to be solved on the impedance control. Within this impedance force control framework, many efforts have been made to solve these problems. Contact stability of the impedance control for stable execution of tasks has been analyzed.[23] In addition to those efforts, various control algorithms have been proposed. Lasky and Hsia[24] have proposed the inner/outer loop control scheme where the robot dynamics uncertainties are compensated by a robust position control algorithm in the inner loop and estimated environment position is modified using an integral control of the force-tracking error in the outer loop. The generalized impedance control of considering a general dynamic relation between a position error and a force error to deal with the unknown environment stiffness has been proposed.[25] The adaptive techniques of using force-tracking errors have been proposed to estimate environment stiffness or adjust controller gains to compensate for unknown environment stiffness.[24] They[24] have proposed a simple trajectory modification scheme using the robot controller to compensate for robot dynamics uncertainties as in ref. [26] and environment stiffness is replaced by contact force information.[25] Later analysis has shown that accurate force-tracking is not always guaranteed unless the accuracy of the estimated environment position is within certain bounds.[27] Further than that[27] have proposed an intelligent force control algorithm using a neural network to compensate for uncertainties.[28] Fuzzy-neuro techniques have been used for force control of unknown objects.[29] The adaptive technique has been used to minimize the force error directly.[30]

Although the force-tracking problem can be solved through modification of the impedance formulation, the other problem relating with unknown environment such as model estimation and environment position still remains to be solved. Exact modeling of an environment helps the impedance function perform well. However, the exact estimation of the environment is a quite difficult process in real situation. In addition to that, the environment position is not available accurately in advance. Poorly estimated information about the environment may yield poor force-tracking results.

The purpose of this paper is to provide a simple solution to the force-tracking impedance control algorithm that is robust with respect to uncertainties in both robot dynamic model and environment position and stiffness. The main idea is to minimize the force error directly by using a simple adaptive gain when tracking unknown environment. Environment stiffness knowledge is not required by the algorithm. The proposed control law is very simple, so that it can be easily implemented in real robot control systems. A five-fingered anthropomorphic artificial hand with multi-sensory and FPGA-based control hardware and software architecture is designed to fulfill the requirements of the grasping-force controller. In order to improve the force-tracking precision, the indirect adaptive algorithm was applied to estimate the parameters of the environment. The generalized momentum-based disturbance observer was applied to estimate the contact force from the torque sensor. Based on the sensors of the finger, an adaptive sliding mode friction compensation algorithm was utilized to improve the accuracy of the position control. Based on the characteristic of the exponential form friction, the sliding mode control law including the estimation of friction parameter is obtained through terminal sliding mode idea, and the on-line parameter update laws are obtained based on Lyapunov stability theorem.

2. Multi-Fingered Robot Hand Systems

2.1. Mechanical design

Since the multi-fingered robot artificial hand intend to use as prosthesis, the hand's anthropomorphic characters (such as the humanoid appearance, the power, and the weight), the grasp functionality, as

https://doi.org/10.1017/S0263574714002161 Published online by Cambridge University Press



Fig. 1. The multi-fingered robot artificial hand system.

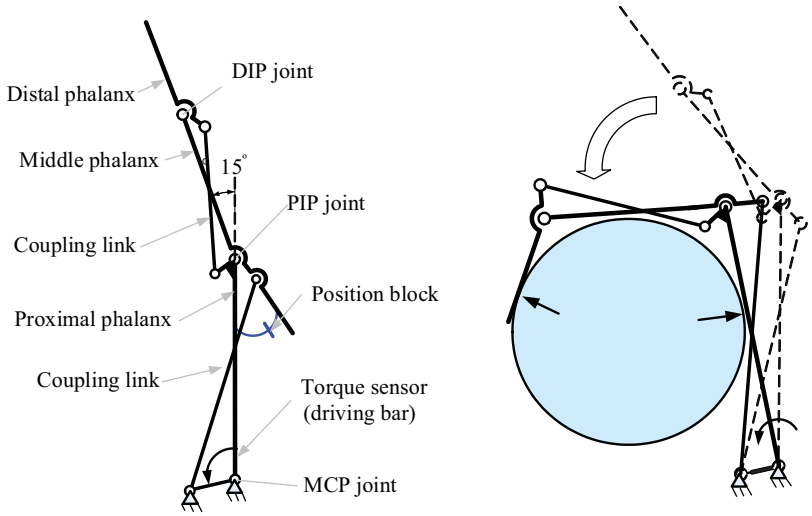


Fig. 2. Kinematics scheme of index finger, mid finger, ring finger, and little finger.

well as the sensor feedback and control should be all taken into account as important criteria. We consider the hand's humanoid appearance in its mechanical design, making the shapes of the palm and fingers, as well as their relative positions, directly featured with the mechanical structure. This endows the hand with superior appearance standalone without extra cover design. The ultimate goal of the mechanical design was to develop a five-fingered hand smaller (nearly 85%) than a normal healthy hand (Asian male), with totally built-in actuation mechanism. The size of prosthetic hand is nearly 159 mm × 79 mm, and 21 mm in thickness (palm), as shown in Fig. 1. The fingers of the hand, which possess three phalanxes each, can be individually actuated. Modular elements, whatever mechanical or electrical, should also be addressed to simplify the system constitution and thus to make maintenance flexible.

For acquiring a great modular interchangeability, the hand's last four digits (index, middle, ring, and little) are designed with the same mechanical structure. Different from commercial prosthesis that use rigid fingers to reduce the transmission complexity, which brings unnatural finger motions and inadequate sensory information, we intend to develop a flexible hand with 15 movable joints (three joints for each finger), as to supply the hand with superior grasp compliance and robustness according to the physiology of human hand. The coupling link mechanism was adopted during the design of finger. In general, two groups of planar linkage mechanism in series, without any elastic parts, were adopted. The motion is transmitted from the motor unit to the coupling linkage mechanism through bevel gears. To imitate the neutral gesture, an initial inflexed angel of 15° was applied between proximal phalanx and medial phalanx, as shown in Fig. 2.

https://doi.org/10.1017/S0263574714002161 Published online by Cambridge University Press

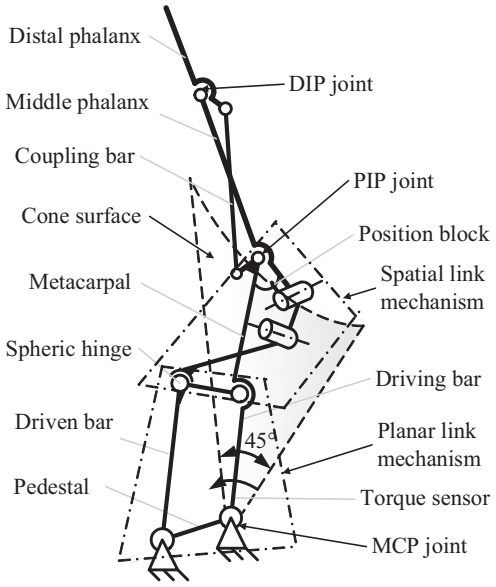


Fig. 3. Kinematics scheme of the thumb.

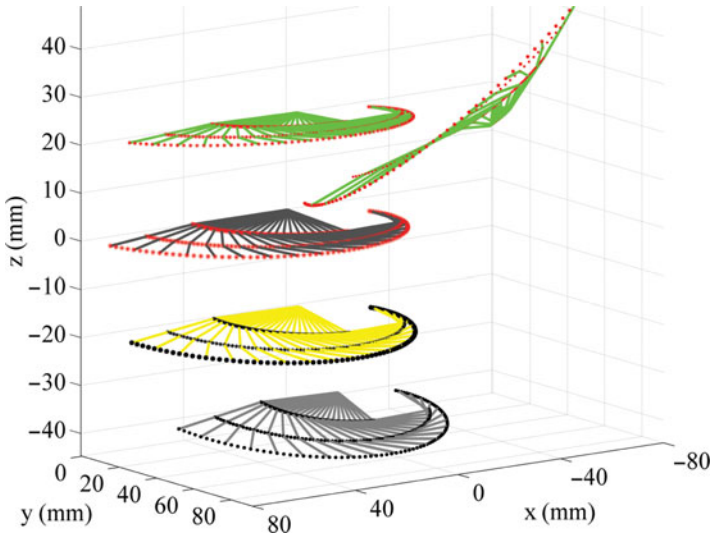


Fig. 4. The operational space of the anthropomorphic artificial hand.

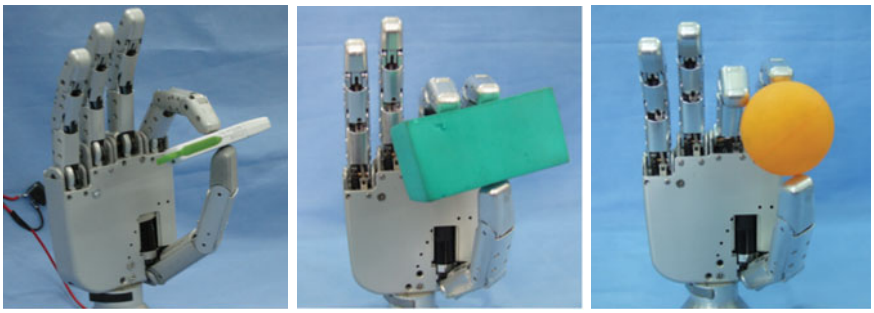
The thumb finger mechanism is also coupled as the other four fingers. As the spheric hinge is bulk, there is not enough room for the spatial link mechanism in kinematics. A quadrilateral four-bar mechanism is applied to drive up the spheric hinge, as shown in Fig. 3. By doing so, the planar finger motion was extended to three-dimensional spaces. The last two joints are coupled as other four fingers. The workspace of thumb presents a cone surface, as shown in Fig. 4.

The experiments of nipping, fisting, and grasping are shown in Figs. 5(a)–(e). It is obvious that the thumb, moving along a cone surface, and other fingers' grasp and appearance resemble human hand, with strong functions.

2.2. Hardware and software architecture

The control system of anthropomorphic artificial hand has to satisfy the conditions of small size, light weight, low power consumption, high computation speed and is integrated into the palm. In an advance bionic prosthesis, the electronic architecture has to be flexible enough to support the real-time control of five active axes, real-time identification of external commands, and computation of control loops and delivering of sensory biofeedback. We consider embedding the mechanical parts, electronics,

https://doi.org/10.1017/S0263574714002161 Published online by Cambridge University Press



(a) Nipping (b) Three-jaw chuck (square) (c) Three-jaw chuck (spherical)



(d) Cylindrical grasp (e) Hook grasp

Fig. 5. The experiments of hand grasping: (a) Nipping, (b) Three-jaw chuck (square), (c) Three-jaw chuck (spherical), (d) Cylindrical grasp, and (e) Hook grasp.

and control totally in the hand, for achieving a modular myoelectric prosthesis that can be easily maintained and thus suitable for a large population of potential users. The modular design concept is wildly applied the mechanical par and the electrical design. The motion control system integrated in the mechanical hand is composed of a motion control subsystem and several sensory subsystems.

For the motion control, the mechanical hand is controlled by an embedded multi-processor controller structured on FPGA. The Electromyography (EMG) controller and the electrical stimulator take charge of decoding the motion intent and providing the sensory feedback, respectively. For easy adjustment, these two parts are not contained in the hand body. The FPGA-based control system is shown in Fig. 6. The A/D port is typically used to sample the torque and the position signals. The Controller Area Network (CAN) port is used to realize the communication with the EMG controller. The serial communications port (SCI) module is used for debugging with power computer (PC) that uses RS-232 protocol. The Pulse Width Modulation (PWM) port is used to drive the H-Bridge chip circuitry. Three H-Bridge drive chips with internal control logic are integrated to drive the five DC motors. The control system communicates with PC by Universal Serial Bus (USB) bus (USB 2.0 480 Mbit/s), and the power can supply by USB electric cable.

The fully embedded torque and position sensors endow the hand with many intelligent control schemes. The sensory subsystem is crucial both for sensory feedback and autonomous operation. A number of sensors like joint angle sensors, torque sensors, and incremental magnetic encoders are integrated in the system. The position control of the finger can be achieved by means of absolute angle sensor (based on Giant Magneto Resistive (GMR) effect) embedded in the metacarpophalangeal (MCP) joint. Small size and contactless working principle can make the GMR-effect sensor to avoid much friction force, and thus provide more accurate information about the joint position to decrease the influence of elasticity and hysteresis of the transmission system. The position precision can reach to 0.04 rad after calibration.

To measure the torque applied on the finger and protect the mechanical structure from overload, a type of one-dimensional torque sensor was integrated into each finger with exception of the little finger. The torque measurement is performed based on strain gauges located on the mechanical elastic structure between the output bevel gear and the actuating linkage. The analog signals were digitally

https://doi.org/10.1017/S0263574714002161 Published online by Cambridge University Press

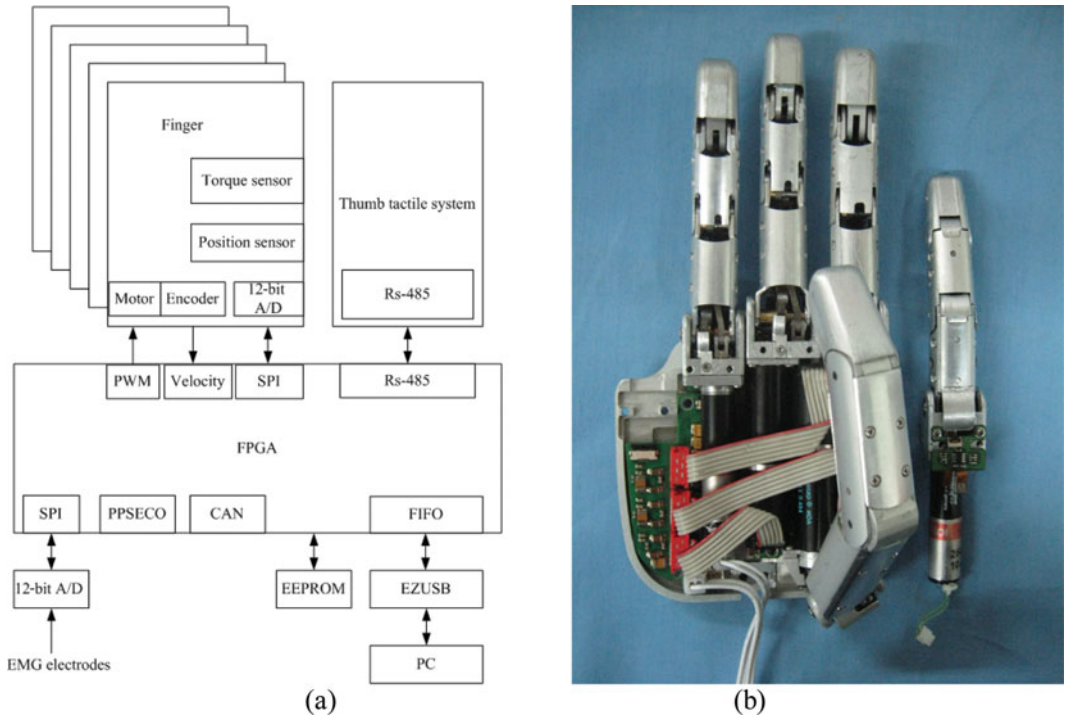


Fig. 6. The multi-fingered robotic hand control architecture based on FPGA.

converted nearby to decrease the electromagnetic disturbance. Then, they were transferred to the motion controller through the flexible connecting board. The sampling frequency of the A/D is set to 500 Hz. The position and torque sensors embedded in the mechanical structure are shown in Fig. 7. The force precision can reach to 0.2 N, which meets to the prosthesis usage.

3. Adaptive Impedance Control for Unknown Environment

3.1. Force-tracking impedance control

Impedance control utilizes a single control law, which attempts to regulate both position and force by specifying a dynamic relationship between them. This relationship is chosen to be a second-order linear impedance because such systems are well understood and simple to control. The standard impedance control law is shown in Eq. (1), where m_t, b_t, k_t are the target impedance mass, damping, and stiffness, x_t is the reference trajectory, x is the actual trajectory, and f_e is the extern force applied to the finger.

$$m_t(\ddot{x} - \ddot{x}_t) + b_t(\dot{x} - \dot{x}_t) + k_t(x - x_t) = f_e \tag{1}$$

The target impedance parameters are specified by the user and have the dimensions of the task space. They cause the finger to exhibit the dynamics of a multi-directional mass–spring–damper system. The target impedance matrices are typically chosen to be diagonal, resulting in uncoupled response along each principle direction of x.

When the finger contacts the environment, a reaction force results which can be defined as

$$f_e = k_e(x_e - x) \tag{2}$$

Here, k_e represents the stiffness characteristics of environment, while x_e represents the environment location (Fig. 8).

In order to achieve the impedance force control, bring reference force f_t into Eq. (1) yields

$$m_t(\ddot{x} - \ddot{x}_t) + b_t(\dot{x} - \dot{x}_t) + k_t(x - x_t) = f_t - f_e \tag{3}$$

https://doi.org/10.1017/S0263574714002161 Published online by Cambridge University Press

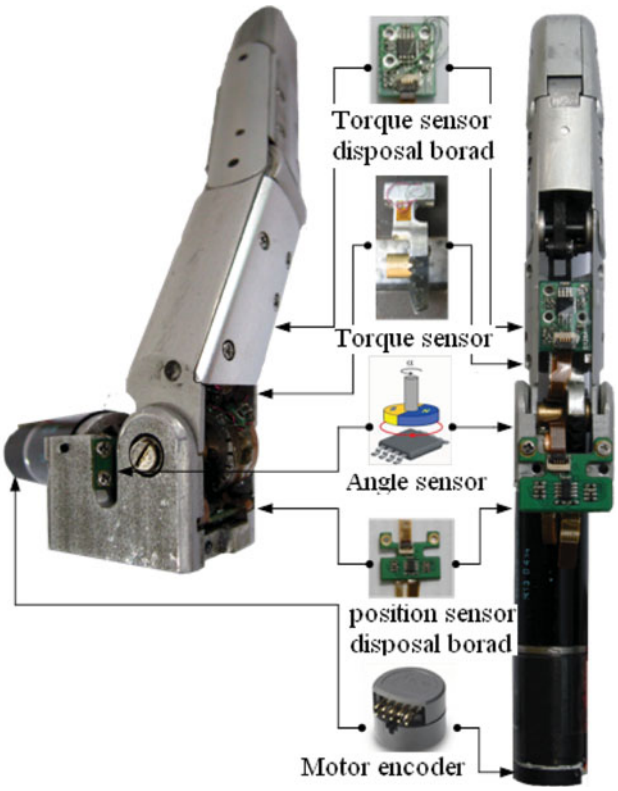


Fig. 7. Torque and position sensors on base joint.

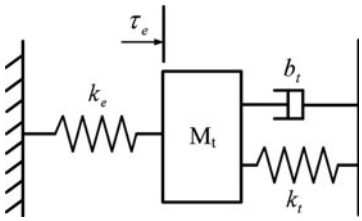


Fig. 8. Contact model of robot and environment.

Combining Eq. (3) with Eq. (2) yields the steady-state force-tracking error is

$$e_{fss} = \frac{kk_e}{k + k_e}\left[\frac{f_t}{k_e} + x_e - x_t\right] \tag{4}$$

From the above, the grasping force-tracking f_t as $e_{fss} = 0$. Regulating grasping force to track a desired force f_t, x_t must be appropriately designed based on f_t, x_e, k_e, and k as follows

$$\frac{f_t}{k_e} + x_e = x_t \tag{5}$$

Therefore, when the environment stiffness k_e and environment location x_e are known exactly, it is straightforward to calculate the reference trajectory x_t from Eq. (5). In practice, it is difficult to know k_e and x_e exactly. In Section 3.3, we propose an indirect adaptive algorithm to estimate k_e and x_e.

3.2. The generalized momentum-based disturbance observer

In order to improve the quality of the force signal, the generalized momentum-based disturbance observer was applied to estimate the contact force from the joint torque sensor.

https://doi.org/10.1017/S0263574714002161 Published online by Cambridge University Press

When the finger contacts the environment, the dynamics mode can be defined as

$$M(\theta)\ddot{\theta} + C(\theta, \dot{\theta})\dot{\theta} + G(\theta) = \tau + J^{\mathrm{T}}(\theta) f_e \tag{6}$$

where $M(\theta)$, $C(\theta, \dot{\theta})$, and $G(\theta)$ represent the inertia matrices, centrifugal term, and gravity term, respectively. τ and $J^{\mathrm{T}}(\theta)$ are control input torque vector and finger's Jacobian, respectively.

Define $J^{\mathrm{T}}(\theta) f_e$ as the disturb torque τ_d, then Eq. (6) can be rewritten as

$$M(\theta)\ddot{\theta} + C(\theta, \dot{\theta})\dot{\theta} + G(\theta) = \tau + \tau_d \tag{7}$$

Define the generalized momentum of the finger as

$$P = M(\theta)\dot{\theta} \tag{8}$$

Differentiating Eq. (8) with respect to time yields

$$\dot{P} = M(\theta)\ddot{\theta} + \dot{M}(\theta)\dot{\theta} \tag{9}$$

Substituting Eq. (7) into Eq. (9) yields

$$\dot{P} = \tau - C(\theta, \dot{\theta})\dot{\theta} - G(\theta) + \tau_d + \dot{M}(\theta)\dot{\theta} \tag{10}$$

Note that $C(\theta, \dot{\theta})$ have the follow characteristic

$$\dot{M}(\theta) = C(\theta, \dot{\theta}) + C^T(\theta, \dot{\theta}) \tag{11}$$

Combining Eqs. (10) and (11) yields

$$\dot{P} = \tau + C^T(\theta, \dot{\theta})\dot{\theta} - G(\theta) + \tau_d \tag{12}$$

Define estimate error as

$$e = P - \widehat{P} \tag{13}$$

where $\widehat{P}$ is estimate value of P.

Differentiating $\widehat{P}$ with respect to time yields

$$\dot{\widehat{P}} = \tau + C^T(\theta, \dot{\theta})\dot{\theta} - G(\theta) + K \times e \tag{14}$$

where K is symmetric, positive-definite matrix. Define υ as $\upsilon = K \times e$, we have

$$\dot{\upsilon} = K(\dot{P} - \dot{\widehat{P}}) = K(\tau_d - \upsilon) \tag{15}$$

By integrating $\widehat{P}$ over time yields

$$\upsilon = K(P - \widehat{P}) = K\left(P - \int_0^t (\tau + C^T(\theta, \dot{\theta})\dot{\theta} - G(\theta) + \upsilon)dt\right) \tag{16}$$

Then, the estimate value of f_e is given by

$$f_e = (J^T(\theta))^{-1}\upsilon \tag{17}$$

https://doi.org/10.1017/S0263574714002161 Published online by Cambridge University Press

3.3. Environmental parameters adaptive estimation technique (EPAEG)

In order to improve the force-tracking precision, the indirect adaptive algorithm[31] was applied to estimate the parameters of the environment. From Eq. (2), the estimate value of the environment react force is

$$\hat{f}_e = \hat{k}_e(\hat{x}_e - x) \tag{18}$$

Combining Eq. (2) and Eq. (18) yields the error of environment react force is

$$e_f = \hat{f}_e - f_e = [-x, 1]\begin{bmatrix} \hat{k}_e - k_e \\ \hat{k}_e\hat{x}_e - k_e x_e \end{bmatrix} \tag{19}$$

If $e_f = 0$ as time $t \to \infty$ can be achieved, $\hat{k}_e \to k_e$ and $\hat{x}_e \to x_e$ are achieved. Define η_e and k_x as

$$\begin{cases} \eta_e = [k_e, k_e x_e]^T \\ k_x = k_e x_e \end{cases} \tag{20}$$

From Eq. (20), we have

$$\hat{\eta}_e = \left[\hat{k}_e, \hat{k}_e\hat{x}_e\right]^T \tag{21}$$

where $\hat{\eta}_e$ is estimate parameter of η_e.

From Eq. (20) and Eq. (21), Eq. (19) can be rewritten as

$$\begin{cases} e_f = [-x, 1]\,\tilde{\eta}_e \\ \tilde{\eta}_e = \hat{\eta}_e - \eta_e \end{cases} \tag{22}$$

Define a Lyapunov function candidate as

$$V_e = \frac{1}{2}\tilde{\eta}_e^T \Gamma_e \tilde{\eta}_e \tag{23}$$

where $\Gamma_e = \mathrm{diag}[\gamma_{e1}, \gamma_{e2}]$ is symmetric, positive-definite matrix, η_e is constant. Differentiating Eq. (23) with respect to time yields

$$\dot{V}_e = \tilde{\eta}_e^T \Gamma_e \dot{\hat{\eta}}_e \tag{24}$$

Define the adaptive laws as

$$\dot{\hat{\eta}}_e = -\Gamma_e^{-1}[-x, 1]^T e_f \tag{25}$$

Combining Eq. (24) and Eq. (25) yields

$$\dot{V}_e = -(\hat{f}_e - f_e)^2 \le 0 \tag{26}$$

Then, the adaptive parameters estimate laws of the environment are given by

$$\begin{cases} \dot{\hat{k}}_e = \gamma_{e1} x \left(\hat{f}_e - f_e\right) \\ \dot{\hat{x}}_e = \dfrac{\left(\hat{f}_e - f_e\right)}{\hat{k}_e}\left(-\gamma_{e2} - \gamma_{e1} x \hat{x}_e\right) \end{cases} \tag{27}$$

https://doi.org/10.1017/S0263574714002161 Published online by Cambridge University Press

3.4. Position control with adaptive sliding mode friction compensations
The mode of the anthropomorphic artificial hand finger can be expressed as

$$\begin{aligned}\frac{d\theta(t)}{dt} &= \omega(t)\\ \frac{d\omega(t)}{dt} &= \frac{1}{T}\omega(t) + \frac{K_o \times K_\theta}{T}U - \frac{K \times K_\theta}{T}T_f\end{aligned} \tag{28}$$

where θ is finger driver motor output angle, ω is finger driver motor angle velocity, U is control system input (the input voltage of finger driver motor), T is electrical time constant of finger driver motor, K_o is open-loop gain of finger servo system, T_f is nonlinear friction torque of finger system, and K_θ is finger drive ratio.

The finger joint angle error $e(t)$ is given by

$$e(t) = \theta_d(t) - \theta(t) \tag{29}$$

where $\theta_d(t)$ and $\theta(t)$ are desired finger joint angle and actual finger joint angle, respectively.

In servo systems, steady-state errors and tracking errors are mainly caused by static friction, which depends on the velocity and payload. The nonlinear friction model is given by

$$T_f(\dot{\theta}) = T_c\dot{\theta} + T_s \times \text{sign}(\dot{\theta}) \tag{30}$$

where T_c and T_s are viscous friction coefficient and static friction coefficient, respectively. And T_c and T_s are estimates by friction observe experiment.[14]

Define $a = \frac{1}{K_o \times K_\theta}$ and $b = \frac{T}{K_o \times K_\theta}$, then

$$\ddot{\theta}(t) = \frac{a\dot{\theta}(t) + U - T_f}{b} \tag{31}$$

Terminal sliding surface is given by

$$s(t) = ce^{q \cdot p} + \dot{e} \tag{32}$$

where c is a positive constant; p and q are positive odd numbers, satisfying $q < p$.

The period of control system that reaches to $e = 0$ on the sliding surface is given by

$$t_s = \frac{p}{c(p-q)}\,|e(\theta)|^{(p-q)/p} \tag{33}$$

where $e^{-a|\dot{\theta}|}$ satisfies $0 < e^{-a|\dot{\theta}|} \leq 1$, and then

$$\left|(T_s - T_c)^{-a|\dot{\theta}|}\text{sign}(\dot{\theta})\right| \leq T_{fm} \tag{34}$$

where T_{fm} is the maximum of interference.

The adaptive sliding mode control law is given by

$$U = -\hat{a}\dot{\theta} - \hat{b}u_c + \hat{T}_c \times \dot{\theta} + \hat{T}_{fm} \times \text{sign}(s_\Delta(t)) \tag{35}$$

where $\hat{a}$, $\hat{b}$, $\hat{T}_c$, and $\hat{T}_{fm}$ are estimate parameters of a, b, T_c, and T_{fm}, respectively; u_c is the auxiliary control input, $s_\Delta(t)$ is the extension function of $s(t)$, and $s_\Delta(t)$ is given by

$$s_\Delta(t) = s(t) - \delta \times \text{sat}\left(\frac{s(t)}{\delta}\right) \tag{36}$$

https://doi.org/10.1017/S0263574714002161 Published online by Cambridge University Press

where δ is the boundary layer coefficient; sat$(\cdot)$ is saturation function and given by

$$\text{sat}(x) = \begin{cases} x \\ \text{sign}(x) \end{cases} \tag{37}$$

Combining Eq. (36) with Eq. (37) yields

$$\begin{cases} \dot{s}_\Delta = s_\Delta = 0 & |s| < \delta \\ \dot{s}_\Delta = \dot{s}, |s_\Delta| = |s| - \delta & |s| > \delta \end{cases} \tag{38}$$

$$s_\Delta \times \text{sat}\left(\frac{s}{\delta}\right) = |s_\Delta| \tag{39}$$

Combining Eq. (39) with Eq. (32) yields

$$\begin{aligned} \dot{s} = c \times \frac{q}{p} \times e^{\frac{q}{p}-1} \times \dot{e} - \frac{1}{b}[a\dot{\theta} - \hat{a}\dot{\theta} - \hat{b}u_c + \hat{T}_c \times \dot{\theta} \\ + \hat{T}_{fm} \times \text{sign}(s_\Delta) - T_c \times \dot{\theta} - T_s \times \text{sign}(\dot{\theta})] \end{aligned} \tag{40}$$

The auxiliary control input u_c is given by

$$u_c = -c \times \frac{q}{p} \times e^{\frac{q}{p}-1} \times \dot{e} - \ddot{r} - \beta \times s_\Delta \tag{41}$$

where β is a positive constant.

The adaptive laws is given by

$$\begin{cases} \dot{\hat{a}} = -\eta_1 \times \dot{\theta} \times s_\Delta \\ \dot{\hat{b}} = -\eta_2 \times u_c \times s_\Delta \\ \dot{\hat{T}}_c = \eta_3 \times s_\Delta \times \text{sign}(\dot{\theta}) \\ \dot{\hat{T}}_{fm} = \eta_4 \times |s_\Delta| \end{cases} \tag{42}$$

where η_1, η_2, η_3, and η_4 are adaptive law gains.

4. Experiment and Discuss

To evaluate the validity of the proposed control experimentally, the adaptive force-tracking impedance control is implemented in a two-dimensional grasp by a five-fingered hand as shown in Fig. 9. Each finger of the hand has three joints with position and torque sensors. The prosthetic hand control system communicates with PC by USB bus (USB 2.0 480 Mbit/s), and the power supply by 6 V. A simple C++ application was written to run on a PC (PC diagnosis in Fig. 9), able to communicate with the hand controller by means of the communication protocol. This application was used to drive the five-finger motor closure and to continuously monitor its base joint position and torque sensors output.

To demonstrate the general validity of the proposed control architectures with the nonlinearity compensation, four experiments using the first two control structures except the adaptive force-tracking impedance control mentioned in Section 3 are executed on our anthropomorphic artificial hand. The experiments are related to three typical application areas for impedance control: the precise force-tracking, the stable and safe interaction of the artificial hand with humans, and contact with unknown, stiff but passive environments. During these experiments, we compare the different control results, and draw conclusions as to their advantages and disadvantages, respectively.

4.1. Friction compensation experiments

Friction compensation experiments are implemented in a single finger. Since friction compensation is achieved in joint space, the experiments of the proposed friction observer are conducted with

https://doi.org/10.1017/S0263574714002161 Published online by Cambridge University Press

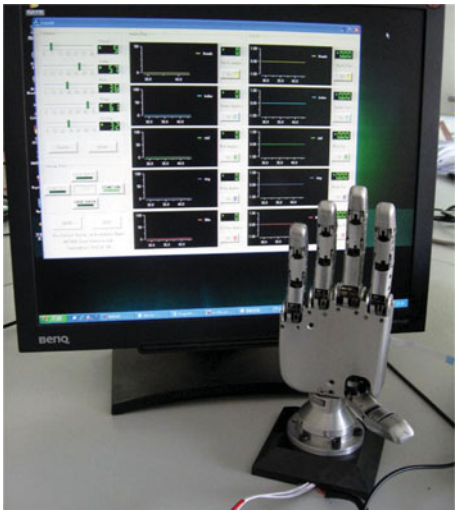


Fig. 9. Experimental platform.

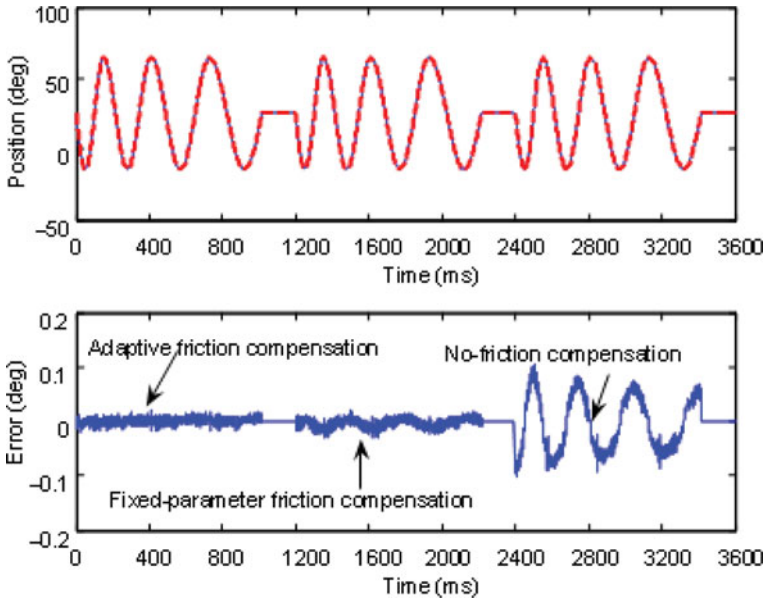


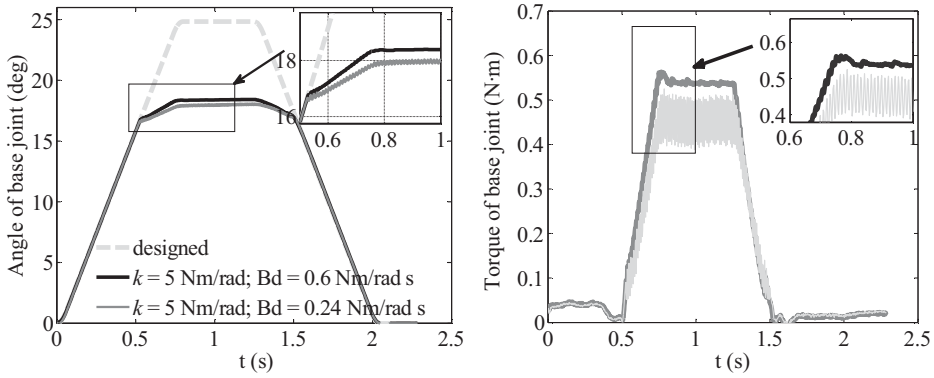
Fig. 10. Position-tracking ability with adaptive, fixed-parameter, and without friction compensation control.

a joint impedance controller as Eq. (1). The control gains for finger are: $K = 80$, $\Gamma_e = \text{diag}\{8\}$, $c = 2$, $p = 3$, $q = 5$, $\delta = 0.8$, $\beta = 2$, $\eta_1 = 0.2$, $\eta_2 = 0.1$, $\eta_3 = 0.1$, $\eta_4 = 0.04$. As shown in Fig. 5, the joint tracks the variable frequency sine curve in free space by adaptive impedance controller, fixed-parameter impedance controller, and no-friction impedance controller. The position error is less than 0.03° with adaptive friction comparing favorably to 0.12° without friction compensation, and 0.06° for fixed-parameters friction. Thus, it can be concluded that improved performance is achieved by the proposed impedance controller with friction observer. Furthermore, adaptive friction compensation control shows that no stick-slip behavior is observed, which demonstrates the feasibility of the adaptive joint friction compensation (Fig. 10).

4.2. The compare experiment of impedance control and adaptive force-tracking impedance control

To demonstrate the general validity of the proposed adaptive force-tracking impedance control architectures with the friction compensation, three sets of experiments using impedance control

https://doi.org/10.1017/S0263574714002161 Published online by Cambridge University Press



(a) Position response in finger joint (b) Torque response in finger joint

Fig. 11. Experimental results of position-based joint impedance control: (a) Position response in finger joint and (b) Torque response in finger joint.

as Eq. (1) and adaptive force-tracking impedance control as Section 3 are conducted to verify the force-tracking impedance control capabilities for unknown environments position.

4.2.1. Joint impedance control. In this section, the experiments of the impedance controller as Eq. (1) are conducted in joint space. The joint impedance control experiment has been made on an index finger of the robot hand, while the other fingers are broken. The robot hand to be grasped is a cylinder with a diameter of 300 mm. Due to the symmetry of the index finger and thumb, only the index finger is employed to demonstrate the effectiveness of the proposed control scheme, whereas the thumb acts as a passive finger in the experiments.

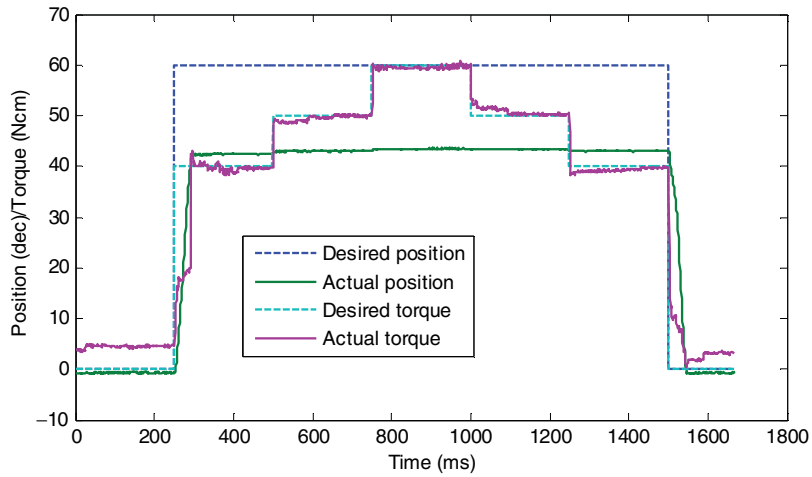
In this experiment, the commanded values of the desired impedance stiffness and damping are different, so that different compliant behaviors are displayed. Figure 11 shows the joint impedance control experiments based on the some stiffness with different damping. As shown in Fig. 11, contact is made with a rigid external object at joint angles of 16°, where real tracking separates from the desired tracking. The experimental results demonstrate that the joints can follow the desired trajectory closely in the free space, and the joint torques increase stably as the fingers make contact with the environment. As shown in Fig. 11, the impedance control fails to track desired force, and the force varies with different target impedance parameters.

4.2.2. Step grasping force-tracking experiment. The adaptive force-tracking impedance control experiment has been made on a single finger of the robot hand, while the other fingers are broken. The position reference has been $x_d = 60°$, which resulted to a collision with a environments surface. During the contact phase, the force reference is changed, as shown in Fig. 12. The finger tracks x_d up to the contact surface, behaving as a position-limited force controller. After impact, as the desired position originates a strong interaction with the environment, contact force is regulated. Changes of force reference are tracked, as long as they have an attainable value. Position tracking is regained when the finger returns into free space.

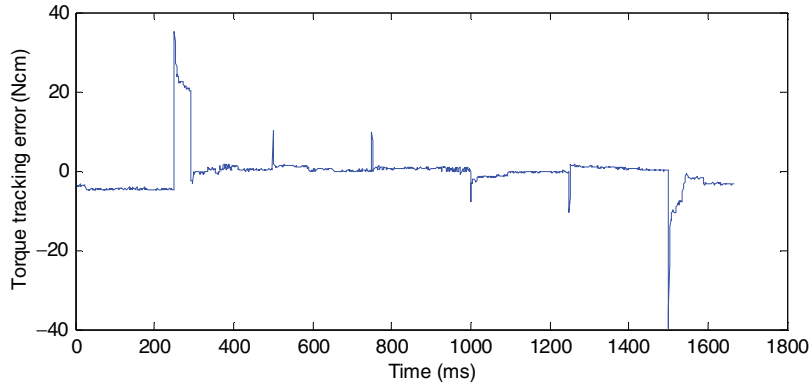
Figures 12(a) and 12(b) illustrate actual grasping force (solid lines) following desired step grasping force (dashdot lines) of the finger and the position error, respectively. The results of the experiment showed the effectiveness of the proposed grasping force control method. The proposed grasping force controller exhibits much smaller force errors (see Fig. 12(b)), while a quite smooth grasping force track is obtained, it can be seen that small force over shoot just after contact and desired grasping force step changed is reached.

4.2.3. Continuous grasping force-tracking experiment. Figures 13(a) and 13(b) illustrate actual grasping force (solid lines) following desired continuous grasping force (dashdot lines) of the finger and the position error, respectively. The results of the experiment showed the effectiveness of the proposed grasping force control method. The proposed grasping force controller exhibits much smaller force errors (see Fig. 13(b)), while a quite smooth grasping force track is obtained, it can be seen that small force over shoot just after contact was reached.

https://doi.org/10.1017/S0263574714002161 Published online by Cambridge University Press



(a) Grasping force tracking



(b) Grasping force tracking errors

Fig. 12. Step grasping force-tracking experiment: (a) Grasping force-tracking and (b) Grasping force-tracking errors.

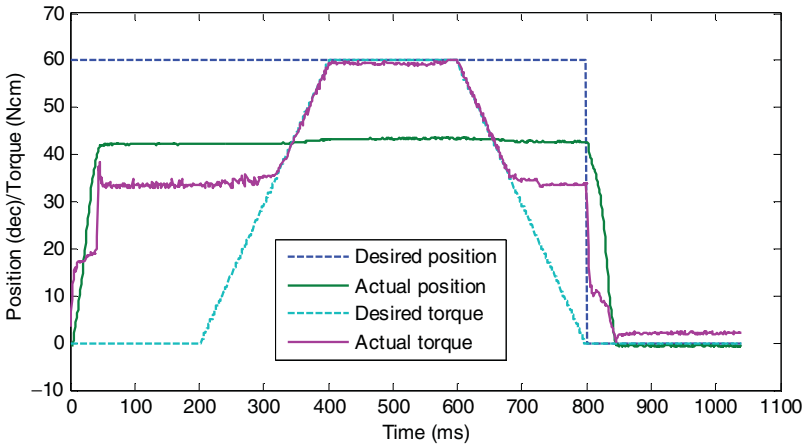
From the compare experiment, we can conclude that the proposed control strategy can solve the force-tracking problem of the impedance control. The proposed controller can adapted to an unknown environment position, the adaptive force-tracking impedance controller can achieve a stable force-tracking through real-time adjust the controller parameters by EPAEG. There will be some impact during the contact phase due to not using trajectory planning and velocity planning. After impact, as the controller real-time estimates the environment position, contact force is regulated.

4.3. The compare experiment for different stiffness

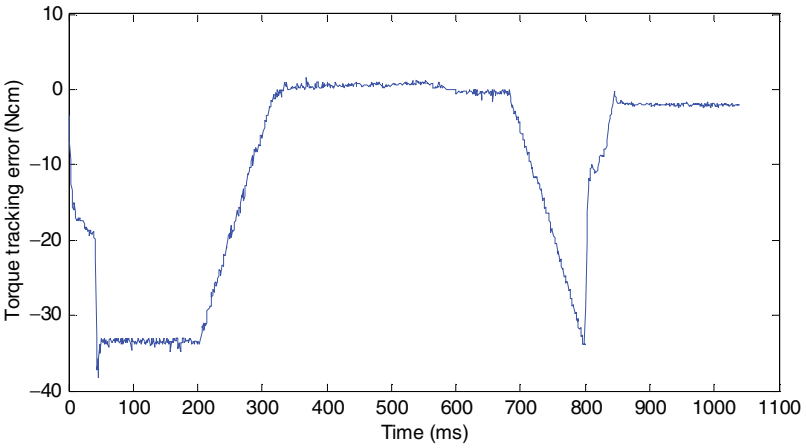
In order to compare the mentioned control strategies more directly, two kinds of compare experiments are performed. One is for testing the performance of EPAEG, the other is for testing the control strategies' robust for different environment stiffness. The control experiment has been made on an index finger of the robot hand, while the other fingers are broken. In order to show the robustness to unknown environment stiffness of the proposed scheme, we tested the system performance for different environment stiffness. In the first experiment, the robot hand to be grasped is a rigid plastic cylinder with a diameter of 450 mm. In the second experiment, the robot hand to be grasped is a soft plastic cylinder with a diameter of 450 mm. Due to the symmetry of the index finger and thumb, only the index finger is employed to demonstrate the effectiveness of the proposed control scheme, whereas the thumb acts as a passive finger in the experiments. In the presented experiment, the position reference has been $x_d = 60^\circ$, which resulted to a collision with a environments surface.

Figures 14(a) and 14(b) illustrate the base joint angle and torque when robot hand grasps rigid plastic cylinder, respectively. As shown in Fig. 14, when the EPAEG is not used, the unstable behavior

https://doi.org/10.1017/S0263574714002161 Published online by Cambridge University Press



(a) Grasping force tracking



(b) Grasping force tracking errors

Fig. 13. Continuous grasping force-tracking experiment: (a) Grasping force-tracking and (b) Grasping force-tracking errors.

of bouncing is observed where the robot finger impacts the rigid plastic cylinder, and the finger fails to track desired force. The adaptive force-tracking impedance controller shows the better performance by minimizing the force-tracking error.

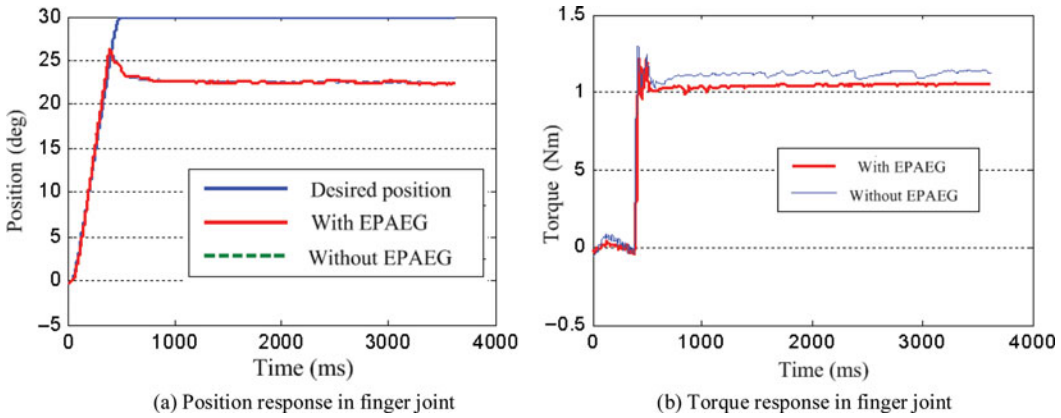
Figures 15(a) and 15(b) illustrate the base joint angle and torque when robot hand grasps soft plastic cylinder, respectively. As shown in Fig. 15, when the EPAEG is not used, the finger enter into the environment is more, and the finger fails to track desired force. When the EPAEG is used, however, the finger enter into the environment is small and the controller shows the better performance by minimizing the force-tracking error.

From the compare experiment, we can conclude that the proposed control strategy can adapt to different environment stiffness. The controller can achieve a stable force-tracking through real-time adjust the controller parameters by environment stiffness adaptive estimated.

5. Conclusion and Future Work

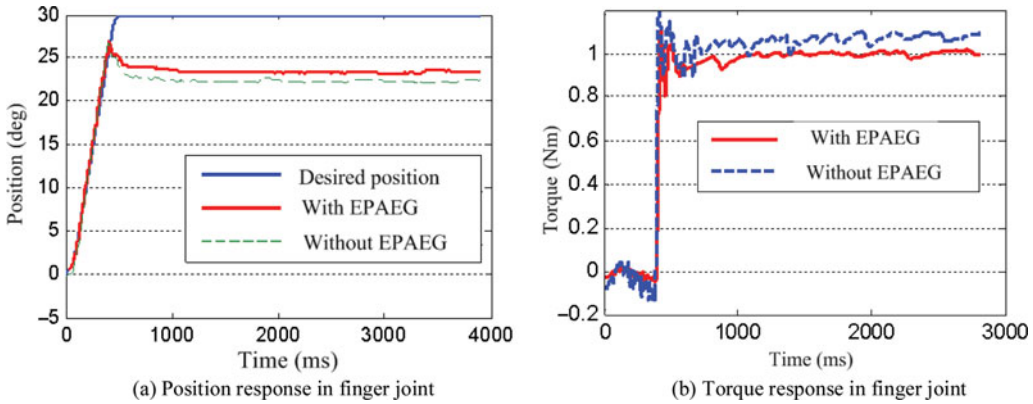
In this paper, the adaptive impedance controllers with adaptive sliding mode friction compensation for anthropomorphic artificial hand are proposed. A five-fingered anthropomorphic artificial hand with multi-sensory and DSP-based control hardware and software architecture is designed to fulfill the requirements of the force-tracking impedance controller. In order to improve the force-tracking precision, the indirect adaptive algorithm was applied to estimate the parameters of the environment. The generalized momentum-based disturbance observer was applied to estimate the

https://doi.org/10.1017/S0263574714002161 Published online by Cambridge University Press



(a) Position response in finger joint (b) Torque response in finger joint

Fig. 14. Contact with rigid plastic: (a) Position response in finger joint and (b) Torque response in finger joint.



(a) Position response in finger joint (b) Torque response in finger joint

Fig. 15. Contact with soft plastic: (a) Position response in finger joint and (b) Torque response in finger joint.

contact force from the torque sensor. Based on the sensors of the finger, an adaptive sliding mode friction compensation algorithm was utilized to improve the accuracy of the position control. The performances of the force-tracking impedance controller and position-based joint impedance control for the five-fingered anthropomorphic artificial hand are analyzed and compared in this paper. Furthermore, the performances of the force-tracking impedance controller with environmental parameters adaptive estimation and without environmental parameters estimation are analyzed and compared. Experimental results prove that accurate force-tracking and stable torque/force response under uncertain environments of unknown stiffness and position can be achieved with the proposed adaptive force-tracking impedance controller with friction compensation on five-finger artificial hand.

The control force is base joint torque sensor of the finger in this paper, we fail to control the actual fingertip force at contact point due to the finger not embed fingertip tactile sensor. In the future, we can real-time control fingertip force using proposed adaptive impedance controller and fingertip tactile sensor to ensure multi-fingered robot hand stable grasping. When humans grasp an object, they use anticipated load conditions plus reflexes based on tactile feedback, to continuously adjust the applied forces. Furthermore, the fingertip three-axis tactile sensor[15,32–34] would be useful for robot hand to be capable of similarly reflexive adjustment to improve their performance.

Acknowledgments

This work was partially supported by the National Program on Key Basic Research Project (973 Program) (2011CB013306), National Natural Foundation of China (51175106, 51205080, 61203346),

https://doi.org/10.1017/S0263574714002161 Published online by Cambridge University Press

Shenzhen Science and Technology Project (ZDSY20120617113312191), Shenzhen Fundamental Research Program (JC201005280481A, JC201105190922A).

References

1. H. Kawasaki, T. Komatsu and K. Uchiyama, "Dexterous anthropomorphic robot hand with distributed tactile sensor: Gifu hand II," *IEEE/ASME Trans. Mechatron.* **7**(3), 296–303 (2002).
2. H. Liu, P. Meusel, G. Hirzinger, M. H. Jin, Y. Liu and Z. W. Xie, "The modular multisensory DLR-HIT-hand: Hardware and software architecture," *IEEE/ASME Trans. Mechatron.* **13**(4), 461–469 (2008).
3. L. Zollo, S. Roccella, E. Guglielmelli, M. C. Carrozza and P. Dario, "Biomechatronic design and control of an anthropomorphic artificial hand for prosthetic and robotic applications," *IEEE/ASME Trans. Mechatron.* **12**(4), 418–429 (2007).
4. J. L. Pons, E. Rocon, R. Ceres, D. Reynaerts, B. Saro, S. Levin and W. V. Moorleghem, "The MANUS-HAND dextrous robotics upper limb prosthesis: Mechanical and manipulation aspects," *Auton. Robots* **16**(2), 143–163 (2004).
5. C. Cipriani, M. Controzzi and M. C. Carrozza, "Objectives, criteria and methods for the design of the SmartHand transradial prosthesis," *Robotica* **28**, 919–927 (2010).
6. M. S. Johannes, J. D. Bigelow, J. M. Burck, S. D. Harshbarger, M. V. Kozlowski and T. V. Dorens, "An overview of the developmental process for the modular prosthetic limb," *Johns Hopkins APL Tech. Dig.* **30**(3), 207–216 (2011).
7. G. X. Li, H. Liu and W. Z. Zhang, "Development of multi-fingered robotic hand with coupled and directly self-adaptive grasp," *Int. J. Humanoid Robot.* **9**(4), 1250034–1–18 (2012).
8. J. L. Pons, R. Ceres and F. Pfeiffer, "Multifingered dextrous robotics hand design and control: A review," *Robotica* **17**, 661–674, (1999).
9. S. Schulz, C. Pylatiuk, M. Reischl, J. Martin, R. Mikut and G. Bretthauer, "A hydraulically driven multifunctional prosthetic hand," *Robotica* **23**, 293–299 (2005).
10. P. Kyberd, C. Light, P. H. Chappell, J. M. Nightingale, D. Whatley and M. Evans, "The design of anthropomorphic prosthetic hands: A study of the southampton hand," *Robotica* **19**, 593–600 (2001).
11. W. Heim, "Microprocessor technology for powered upper extremity prosthetic control systems," *Robotica* **23**, 275–276 (2005).
12. A. Parmiggiani, M. Maggiali, L. Natale, F. Norl, A. Schmitz, N. Tsagarakis, J. S. Victor, F. Becchi, G. Sandini and G. Metta, "The design of the iCub humanoid robot," *Int. J. Humanoid Robot.* **9**(4), 1250027–1–24 (2012).
13. H. Huang, Y. J. Pang, L. Jiang, S. W. Fan, X. Q. Wang and H. Liu, "Underactuated hand dynamic modeling, its real-time simulation, and control," *Int. J. Humanoid Robot.* **7**(4), 609–634 (2010).
14. T. Zhang, L. Jiang and H. Liu, "A novel grasping force control strategy for multi-fingered prosthetic hand," *J. Cent. South Univ.* **19**(6), 1537–1542 (2012).
15. T. Zhang, S. W. Fan, H. Liu and L. Jiang, "Development and experiment analysis of anthropomorphic prosthetic hand with flexible three-axis tactile sensor," *Int. J. Humanoid Robot.* **10**(3), 1350028–1–1350028–24 (2013).
16. M. R. Cutkosky, "On grasp choice, grasp models, and the design of hands for manufacturing tasks," *IEEE Trans. Robot. Autom.* **5**(3), 269–279 (1989).
17. H. Seraji and R. Colbaugh, "Force Tracking in Impedance Control [C]," *IEEE International Conference on Robotics and Automation*, Georgia, IEEE Press (1993), pp. 499–506.
18. N. Hogan, "Impedance control an approach to manipulation. I-Theory. II-Implementation. III-applications," *ASME Trans. J. Dyn. Syst. Meas. Control* (ISSN 0022-0434), **107**, 1–24 (1985).
19. L. Biagiotti, H. Liu, G. Hirzinger and C. Melchiorri, "Cartesian Impedance Control for Dexterous Manipulation," *Proceedings of the IEEE/RSJ International Conference on Intelligent Robots and Systems*, Las Vegas, IEEE Press (2003) pp. 3270–3275.
20. R. Wei, X. Gao, M. Jin, Y. Liu, H. Liu, N. Seitz, R. Gruber and G. Hirzinger, "FPGA based Hardware Architecture for HIT/DLR Hand," *Proceedings of the IEEE/RSJ International Conference on Intelligent Robots and Systems*, Edmonton, IEEE Press (2005) pp. 523–528.
21. D. Erickson, M. Weber and I. Sharf, "Contact stiffness and damping estimation for robotic systems [J]," *Int. J. Robot. Res.* **22**(1), 41–57 (2003).
22. H. Seraji and R. Colbaugh, "Force tracking in impedance control [J]," *Int. J. Robot. Res.* **16**(1), 97–117 (1997).
23. D. Santis, B. Siciliano, A. D. Luca and A. Bicchi, "An atlas of physical human–robot interaction [J]," *Mech. Mach. Theory* **43**, 253–270 (2008).
24. T. Lasky and T. C. Hsia, "On Force-Tracking Impedance Control of Robot Manipulators [C]," *IEEE International Conference on Robotics and Automation*, Sacramento, IEEE Press (1991), pp. 274–280.
25. P. Scherillo, B. Siciliano, L. Zollo, M. Carrozza, M. Guglielmelli and P. Dario, "Parallel Force/Position Control of a Novel Biomechatronic Hand Prosthesis [C]," *IEEE/ASME International Conference on Advanced Intelligent Mechatronics*, Como, IEEE Press (2003), pp. 920–925.
26. S. Jung, T. C. Hsia and R. G. Bonitz, "Force tracking impedance control of robot manipulators under unknown environment [J]," *IEEE Trans. Control Syst. Technol.* **12**(3), 474–483 (2004).

https://doi.org/10.1017/S0263574714002161 Published online by Cambridge University Press

27. G. Dillon and K. Horch, "Direct neural sensory feedback and control of a prosthetic arm [J]," *IEEE Trans. Neural Syst. Rehabil. Eng.* **13**(4), 468–472 (2005).
28. S. Jung, S. B. Yim and T. C. Hsia, "Experimental Studies of Neural Network Impedance Force Control for Robot Manipulators [C]," *IEEE International Conference on Robotics and Automation*, Seoul, IEEE Press (2001), pp. 3453–3458.
29. K. Kiguchi and T. Fukuda, "Position/force control of robot manipulators for geometrically unknown objects using fuzzy neural networks [J]," *IEEE Trans. Ind. Electron.* **47**, 641–649 (2000).
30. S. Jung, T. C. Hsia and R. G. Bonitz, "Force tracking impedance control of robot manipulators under unknown environment [J]," *IEEE Trans. Control Syst. Technol.* **12**(3), 474–483 (2004).
31. C. S. Tzafestas, N. K. Msirdi and N. Manamani, "Adaptive impedance control applied to a pneumatic legged robot [J]," *Int. J. Robot. Res.* **20**(2–4), 105–129 (1997).
32. T. Zhang, H. Liu, L. Jiang, S. Fan and J. Yang, "Development of a flexible 3-D tactile sensor system for anthropomorphic artificial hand," *IEEE Sens. J.* **13**(2), 510–518 (2013).
33. M. Ohka, Y. Mitsuya, I. Higashioka and H. Kabeshita, "An experimental optical three-axis tactile sensor for micro-robots," *Robotica* **23**, 457–465 (2005).
34. M. Ohka, Y. Mitsuya, Y. Matsunaga and S. Takeuchi, "Sensing characteristics of an optical three-axis tactile sensor under combined loading," *Robotica* **22**, 213–221 (2004).

https://doi.org/10.1017/S0263574714002161 Published online by Cambridge University Press